Simulating electromagnetically induced transparency and its potential for quantum computing

Delano Yoder

***Abstract*—In this paper, we investigate the known properties of electromagnetically induced transparency (EIT). EIT offers a unique phenomenon that ultimately allows an atom to experience excitation in a smaller spatial region than the beam's wavelength, overcoming the diffraction limit. EIT is important in quantum computing since it will allow qubits to be packed more closely and increase the rates of two-qubit gate fidelity.**

I. Introduction

QUANTUM computing uses quantum phenomena such as superposition and entanglement to take advantage of an interference property commonly overlooked in the classical world. This property can help quantum computers solve complex problems exponentially faster than classical computers. An essential part of creating interference is entangling qubits with high fidelity. With such a promise, the brightest individuals across the globe are driving quantum computing in many different formats, including superconducting, trapped ions, photons, quantum dots, topological, NV centers, and neutral atoms.

Out of all the current quantum computing formats, neutral atoms seem to have one of the best scenarios for scaling beyond hundreds of qubits, a necessary threshold for useful quantum computing. One approach to scaling would be to decrease the spacing between atoms. A limiting factor for this spacing is the diffraction limit of the electromagnetic fields used to interact with these atoms during computations. EIT can overcome this diffraction limit, allowing for closely packed atom arrays.

Another benefit of using EIT is the application for two-qubit gates. Neutral atom quantum computing uses many different two-qubit gates such as Rydberg dipole-dipole gates used for entanglement, multi-qubit gates, non-classical quantum states, and other two-qubit gates. These gates will see an increase in speed and fidelity due to the coherence of the EIT method and closer spacing of atom arrays. These advantages can help develop neutral atom quantum computing in areas that have been otherwise hindered throughout all quantum computing formats.

II. Three-Level Schemes

Neutral atom quantum computing uses three-level schemes to encode quantum information in an atom's hyperfine states. Two generic three-level schemes are the ladder and vee-type schemes, as seen in figure 1. EIT cannot be induced in the ladder and vee-type schemes since they do not possess the property of a metastable dark state and, therefore, will always decay back to the ground state. Observations of dark states and coherent population trapping (CPT) have been explained in past experiments and give some insight into why a three-level lambda scheme is an ideal choice for EIT [5], [6], as seen in figure 2 [1].

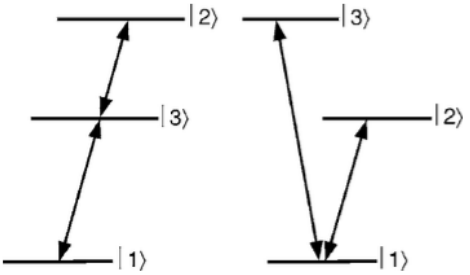

Figure 1: Ladder (left) and vee-type (right) three-level schemes. These do not possess the possibility for useful EIT due to the lack of a metastable state. Figure is taken from [1].

To create an EIT beam, a coupling laser is first turned on, followed by a probe laser that corresponds to the resonant transitions ω_c and ω_p, between $|2\rangle$ to $|3\rangle$ and $|1\rangle$ to $|3\rangle$ respectively. Using relatively slow varying laser pulses, compared to instantaneous rabi frequencies used in other techniques, the population of the excited electronic state becomes negligible, removing the need to keep track of radiative decay.

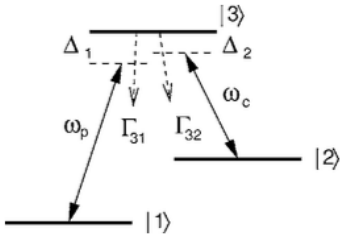

Figure 2: Generic system for EIT: lambda-type scheme with probe field of frequency ω_p and coupling field of frequency ω_c. $\Delta_1 = \omega_{31} - \omega_p$ and $\Delta_2 = \omega_{32} - \omega_c$ denote field detunings from atomic resonances and Γ_{ik} radiative decay rates from state $|i\rangle$ to state $|k\rangle$. Figure is taken from [1].

We can now quantize the atom-laser interaction, within the dipole approximation, in terms of the rabi frequencies associated with our laser beams. Starting with the basic form of the interaction Hamiltonian, seen in equation (1)

$$\tilde{H_{int}} = \mu \cdot E \tag{1}$$

where μ is the transition electronic dipole moment and E is the electric field, we can use a rotating wave approximation

in the unitary transformation to find a more workable interaction Hamiltonian. Equation (2) shows how we transform the Hamiltonian.

$$\tilde{H} = \hat{U}\hat{H}\hat{U}^{\dagger} + i\hbar(\delta_t U)U^{\dagger} \tag{2}$$

δ_t is the Kronecker delta function which is equal to 1 if $t = 0$ and equal to 0 otherwise. Equation (3) shows the generic unitary transformation matrix used in equation (2).

$$\hat{U} = \begin{bmatrix} e^{i\omega_1 t} & 0 & 0 \\ 0 & e^{i(\omega_1+\omega_p-\omega_c)t} & 0 \\ 0 & 0 & e^{i(\omega_1+\omega_p)t} \end{bmatrix} \tag{3}$$

Our three-level atom interaction with the probe and coupling lasers of rabi frequencies Ω_p and Ω_c respectively can then be represented by the interaction Hamiltonian in equation (4). Here we can see how each beam relates to the populations of our three-level system.

$$\bar{H}_{int} = -\frac{\hbar}{2}\begin{bmatrix} 0 & 0 & \Omega_p \\ 0 & -2(\Delta_1 - \Delta_2) & \Omega_c \\ \Omega_p & \Omega_c & -2\Delta_1 \end{bmatrix} \tag{4}$$

Here our detunings are $\Delta_1 = \omega_{31} - \omega_p$ and $\Delta_2 = \omega_{32} - \omega_c$. More details on these calculations can be found in [2] and [3].

III. Dark State Simulation

To simulate the dark states that allow for EIT, we aim to look at the population coefficient equations. To calculate our Hamiltonian we first decompose the terms for the bare atom, H_0, and the interaction Hamiltonian, H_{int}, as seen in equations (5), (6), and (7).

$$H = H_0 + H_{int} \tag{5}$$

$$H_0 = \hbar(\omega_1 |1\rangle \langle 1| + \omega_2 |2\rangle \langle 2| + \omega_3 |3\rangle \langle 3|) \tag{6}$$

$$\begin{aligned} H_{int} = \frac{\hbar}{2}[&(\Omega_p e^{-i\phi_p} e^{-i\nu_p t} |1\rangle \langle 3| + \Omega_c e^{-i\phi_c} e^{-i\nu_c t} |2\rangle \langle 3|) \\ &-(\Omega_p e^{-i\phi_p} e^{-i\nu_p t} |3\rangle \langle 1| + \Omega_c e^{-i\phi_c} e^{-i\nu_c t} |3\rangle \langle 2|)] \end{aligned} \tag{7}$$

Note the rotating wave approximation is accounted for in the interaction Hamiltonian. Using the wavefunction of our three-level system (equation (8)), we can describe our system in the Schrodinger picture.

$$|\Psi(t)\rangle = c_1(t)e^{-i\omega_1 t} + c_2(t)e^{-i\omega_2 t} + c_3(t)e^{-i\omega_3 t} \tag{8}$$

By first simplifying the energies associated with the wavefunction to $\omega_1 = 0$, $\omega_2 = \omega_{12}$, and $\omega_3 = \omega_{13}$ our wavefuntion becomes equation (9).

$$|\Psi(t)\rangle = c_1(t) + c_2(t)e^{-i\omega_{12} t} + c_3(t)e^{-i\omega_{13} t} \tag{9}$$

Using the Schrodinger Equation (10) we can now apply the equations (11) and (12) to obtain our differential equations of the population coefficients.

$$i\hbar\frac{d}{dt}|\Psi\rangle = H|\Psi\rangle \tag{10}$$

$$\begin{aligned} i\hbar\frac{d}{dt}|\Psi\rangle = i\hbar(&\dot{c}_1 + c_1(-i\omega_1)e^{-i\omega_1 t}|1\rangle \\ &+\dot{c}_2 + c_2(-i\omega_2)e^{-i\omega_2 t}|2\rangle \\ &+\dot{c}_3 + c_3(-i\omega_3)e^{-i\omega_3 t}|3\rangle) \end{aligned} \tag{11}$$

$$\begin{aligned} H|\Psi\rangle = \frac{\hbar}{2}(&2\omega_1 c_1 e^{-i\omega_1 t}|1\rangle + 2\omega_2 c_2 e^{-i\omega_2 t}|2\rangle + 2\omega_3 c_3 e^{-i\omega_3 t}|3\rangle \\ &-\Omega_p e^{-i\phi_p} e^{-i\nu_p t} c_1 e^{-i\omega_1 t}|3\rangle - \Omega_c e^{-i\phi_c} e^{-i\nu_c t} c_2 e^{-i\omega_2 t}|3\rangle \\ &-\Omega_p e^{-i\phi_p} e^{-i\nu_p t} c_3 e^{-i\omega_3 t}|1\rangle - \Omega_c e^{-i\phi_c} e^{-i\nu_c t} c_3 e^{-i\omega_3 t}|2\rangle) \end{aligned} \tag{12}$$

By multiplying the bras of each state and with some simplification we can obtain our differential equations (13), (14), and (15).

$$\frac{dc_1}{dt} = \frac{i}{2}\Omega_p e^{i\phi_p} c_3 e^{-i(\omega_{13}-\nu_p)t} \tag{13}$$

$$\frac{dc_2}{dt} = \frac{i}{2}\Omega_c e^{i\phi_c} c_3 e^{-i(\omega_{13}-\omega_{12}-\nu_p)t} \tag{14}$$

$$\frac{dc_3}{dt} = \frac{i}{2}(\Omega_p e^{-i\phi_p} c_1 e^{i(\omega_{13}-\nu_p)t} + \Omega_c e^{-i\phi_c} c_2 e^{i(\omega_{13}-\omega_{12}-\nu_p)t}) \tag{15}$$

Introducing the detunings $\Delta_p = \omega_{13} - \nu_p$ and $\Delta_c = \omega_{13} - \omega_{12} - \nu_p$ we obtain the more simplified differential equations (16), (17), and (18).

$$\frac{dc_1}{dt} = \frac{i}{2}\Omega_p e^{i\phi_p} c_3 e^{-i\Delta_p t} \tag{16}$$

$$\frac{dc_2}{dt} = \frac{i}{2}\Omega_c e^{i\phi_c} c_3 e^{-i\Delta_c t} \tag{17}$$

$$\frac{dc_3}{dt} = \frac{i}{2}(\Omega_p e^{-i\phi_p} c_1 e^{i\Delta_p t} + \Omega_c e^{-i\phi_c} c_2 e^{i\Delta_c t}) \tag{18}$$

Finally, these equations can be further simplified by choosing the phase angle and detunings to be zero, where $\phi_p = \phi_c = 0$ and $\Delta_p = \Delta_c = 0$. These differential equations, (19), (20), and (21), are now the basis for investigating dark states and how varying the timing, spatial relation, and laser intensities can affect our spatial localization of a EIT beam.

$$\dot{c}_1 = \frac{i}{2}\Omega_p c_3 \tag{19}$$

$$\dot{c}_2 = \frac{i}{2}\Omega_c c_3 \tag{20}$$

$$\dot{c}_3 = \frac{i}{2}(\Omega_p c_1 + \Omega_c c_2) \tag{21}$$

More details on these calculations can be found in [2] and [4].

Figure 3 is a simulated dark state where the probe laser and coupling laser intensities are equal. Each laser is initially turned on with a hyperbolic tangent wave shape to prepare the dark state adiabatically. This allows for the system to be insensitive to timing and driving pulse uncertainties [7]. As mentioned before, the coupling laser is turned on to ensure that all of the population is in the ground state before the probe laser is turned on. Both beams will drive the population to the dark state, where the atom becomes transparent. As we see in figure 3 both c_1 and c_2 have a population coefficient of $\frac{1}{\sqrt{2}}$. This quantum interference cancels the absorption experienced by the atom rendering it transparent.

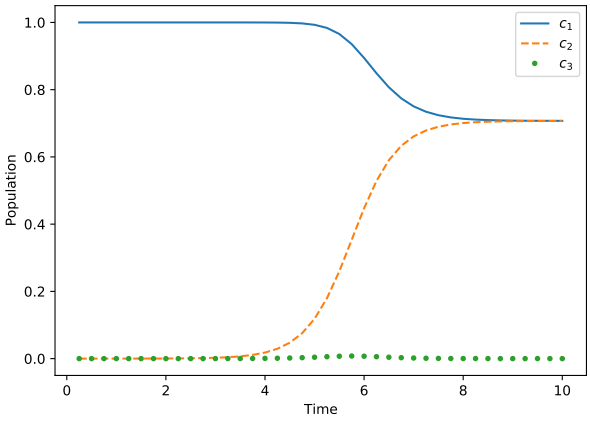

Figure 3: Simulation of a dark state in a three-level lambda scheme. c_1 (blue solid line) is the ground state, c_2 (orange dashed line) is the excited state, and c_3 (green dotted line) is the dark state. The coupling laser was turned on at $t = 1$ and the probe laser was turned on at $t = 6$. The laser intensities were both set to 50 (i.e. $\Omega_p = \Omega_c = 50$). The values for each population were determined by taking the absolute value of each complex differential equations at each time step. All values have been normalized for simplicity.

IV. Other Uses for Dark States

As mentioned before, dark states are susceptible to CPT and also stimulated raman adiabatic passage (STIRAP) [8]. Further more, using EIT one can obtain light that propagates substantially slower known as slow light [9]-[14], and light storage in atomic medium, known as stopped light, that can be used for quantum memory [15]-[20]. One interesting application for the EIT quantum memory technique is its possible use in quantum repeaters. Since quantum communication over long distances will have unavoidable decoherence effects on the associated flying qubits quantum repeaters are necessary. Overall, EIT quantum memory is an attractive solution to storing and retransmitting the quantum information without destroying it.

Additionally, EIT quantum memory has been used in multiple different materials such as warm atomic vapor [21]-[25], Bose-Einstein condensate [26]-[28], and rare-earth doped solid state materials [29]. Like the rest of this paper, EIT quantum memory has been proposed and observed to be highly beneficial in the applications of cold atoms [30]-[38].

V. Electromagnetically Induced Transparency

When thinking about the beam size being smaller than the wavelength, intuitively we think about a point-like beam. It's not so much that the EIT beams are reduced to smaller than their wavelength, but more so that the atom experiences the excitation in a smaller spatial region. This localization of the hyperfine excitations is what's measured to be the beam spatial width that beats the diffraction limit. Past experiments have observed a beam localization that was 8 times smaller, and later 13 times smaller than the beam wavelength [7].

In figure 4 we show how the population transfer differs over the spatial range of a standing wave coupling laser with a spatially uniform probe laser. We see as the coupling beam's rabi frequency amplitude decreases, the population of c_2 increases, up to the point where the rabi frequency amplitude approaches zero and only the probe beam is on. We find that the dark states appear where the coupling beam's amplitude is greatest. We can further shape the population transfer to become more narrow by increasing the maximum amplitude of the coupling beam's rabi frequency relative to the amplitude of the probe beam's rabi frequency. This shows the exponential decrease relationship between the beam amplitude ratios and full width half maximum of the population transfer profile as seen in figure 6.

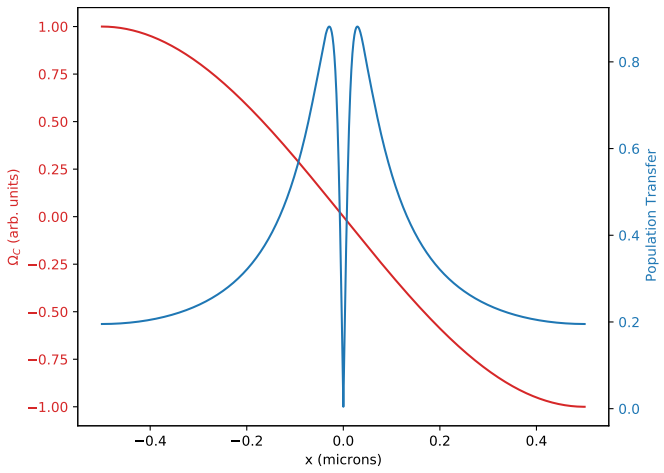

Figure 4: Simulation of the spatial offset from a standing wave coupling beam (red) with a maximum amplitude rabi frequency 5 times greater than that of the probe beam and how it affects the population transfer of the excited state, c_2 (blue). Here we can see an atom at x=0 microns will be excited but a neighboring atom at x=0.5 has a much lower probability of being excited.

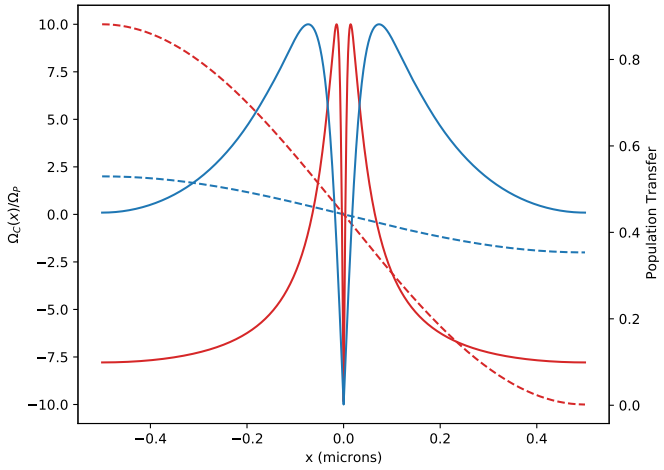

Figure 5: The same simulation as figure 4 of the spatial offset from a standing wave coupling beam (dashed lines) with a maximum amplitude rabi frequency 2 times greater (blue) and 10 times greater (red) than that of the probe beam and how it affects the population transfer of the excited state, c_2 (solid lines).

With an increase in the intensity ratio $|\Omega_c/\Omega_p|$ our excitation window becomes smaller. We can quantize this window to $FWHM_{excitation} \approx \lambda(\Omega_p/\Omega_{c,max})$, where $\Omega_{c,max}$ is the maximum amplitude of the standing wave coupling laser's rabi frequency [7]. This allows for the spacing between atoms to be far shorter than the wavelength allowing for efficient two-qubit gates between atom pairs.

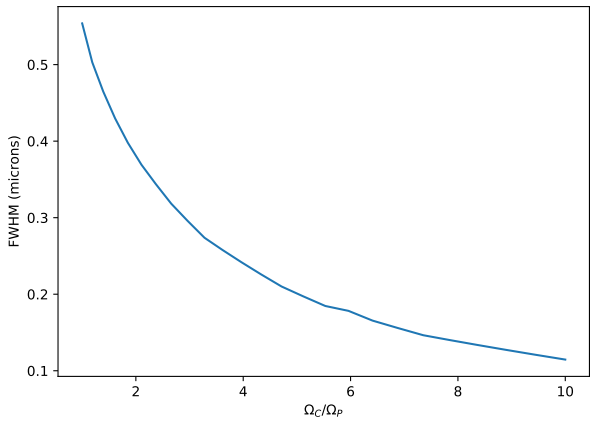

Figure 6: The exponential decrease of the population transfer profile, as seen in figure 4, as we change the maximum amplitude of the coupling beam's rabi frequency. As the intensity of the coupling beam increases relative to the probe beam we see a sharper population transfer profile and a smaller spatial localization window produced by the EIT beams.

VI. EIT Error

When working with experimental results errors should be accounted for. For a two-qubit gate spontaneous emission can be estimated by equation (22)

$$\tau\gamma c_2 \approx \tau\gamma(\Omega_p/\Delta_p) \approx \gamma/\Delta_p \tag{22}$$

where the radiative decay rate of the excited state is 2γ and the detuning of the probe laser is Δ_p. For a non-adiabatic coupling between the dark and excited states the effective rabi frequency in equation (23) [39]

$$\Omega_{NA} \approx \Omega_p/(T\Omega_c) \tag{23}$$

gives a resulting population loss, as seen in equation (24), from the dark state to the excited state on the same order as our spontaneous emission error seen in equation (22)

$$\rho_e \approx (\Omega_{NA}/\Delta_c)^2 \approx (\Omega_p/\Omega_c)^6 \tag{24}$$

where the detuning of the coupling laser is Δ_c. This can be mostly avoided by using the adiabatic approach discussed above. These are the dominant sources of systematic error giving a total error seen in equation (25).

$$P_e \approx (\gamma/\Delta) + (\Omega_p/\Omega_c)^6 \tag{25}$$

There are other sources of error which include Stark shifts and spontaneous emission, but are negligible when compared to the dominant sources derived above. When working with atomic arrays with spacings smaller than the EIT beam wavelength other errors such as dipole-dipole interactions and cooperative decay effects may play a role [40]. Atoms can also experience interactions with the control field due to the finite extent of their wavefunction. The errors seen in table I can be summed to determine what kind of uncertainties to expect [41].

	Error source	Error scaling (P_e)
1	decay error on atom 1	γ/Δ
	localization error on atom 1:	
2	- ions and atoms in fast limit and solid-state qubits [23]	$(\Omega_{ca}/\Omega)^2$
3	- ions and atoms in adiabatic limit	$(\Omega_{ca}/\Omega)^2/(\tau\omega)^4$
4	unitary error on atom 2	$(\Omega/\Omega_c)^6$
5	dipole-dipole error	$(g\Omega/(\Delta\Omega_c))^4$
6	$\|r\rangle$ decay on atom 2 for Rb	$(\Omega/\Omega_c)^2\gamma_r\tau$

Table I: Error budget for the single-qubit phase gate. Taken from [41].

VII. Phase Manipulation

As expected, we can apply a phase shift of the ground state to a spatially localized window as well. In figure 7 we show the same coupling and probe lasers as applied in figure 4, but instead observing the phase of c_1. For a phase change we find a much tighter spatial window than the excitation of c_2. The

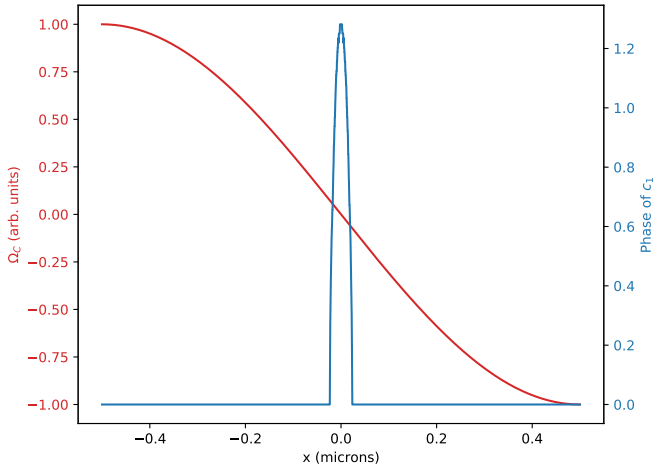

Figure 7: Simulation of the spatial offset from a standing wave coupling beam (red) with a maximum amplitude rabi frequency 5 times greater than that of the probe beam and how it affects the phase of the ground state, c_1 (blue). Here we can see the phase change due to EIT and how this can be used to implement two-qubit phase gates with small spatial windows.

same relationship seen in figure 6 of the intensity ratios and the spatial localization window is seen in figure 8.

Since the spatial localization window of the phase change is small we can use this approach to increase the fidelity of a two-qubit entanglement gate.

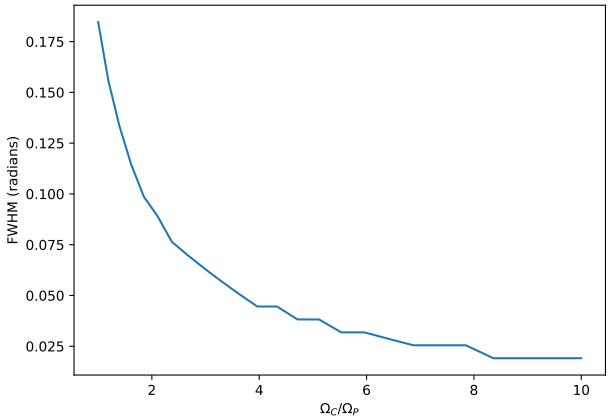

Figure 8: Again we see the exponential decrease of the phase change profile, as seen in figure 7, as we change the maximum amplitude of the coupling beam's rabi frequency. As the intensity of the coupling beam increases relative to the probe beam we see a sharper phase change profile and a smaller spatial localization window produced by the EIT beams while keeping the amplitude of the phase change constant.

VIII. Conclusion

We have presented a summary of simulated dark state EIT beams and they're nonlinear optical effects on a lambda three-level system. In principle this technique can be used to achieve excitations and phase shifts at nanometer spatial widths over nanosecond time scales, increasing both the fidelity and speed of entanglement gates in quantum information technology. This will help solve addressing issues that has prevented the scalability of neutral atom quantum computing.

In practice there are many sources of error to resolve such as spontaneous emission, population losses, and atomic heating [41], [7] to make single-qubit and two-qubit gates reliable enough for quantum computation. Nevertheless, dark state EIT seems to be a promising technique that will help the field of quantum computing move forward.

References

[1] Michael F., Atac I., and Jonathan P. M., "Electromagnetically induced transparency: Optics in coherent media", Rev. Mod. Phys. 77, 633, 2005.
[2] zjs, "Derivation Of Density Matrix Equations, EIT, etc. for 3-level system", [Not Online], 2015.
[3] D. A. Steck, "Quantum and Atom Optics", [Online]. Available: http://atomoptics-nas.uoregon.edu/dsteck/teaching/quantum-optics/quantum-optics-notes.pdf, 2007.
[4] M. Scully and S. Zubairy, "Quantum Optics", Cambridge University Press, 1997. [Online]. Available: http://books.google.com/books?id=20ISsQCKKmQC
[5] Arimondo, E., Orriols, G., "Nonabsorbing atomic coherences by coherent two-photon transitions in a three-level optical pumping", Lett. Nuovo Cimento 17, 333–338, 1976.
[6] H. R. Gray, R. M. Whitley, and C. R. Stroud, "Coherent trapping of atomic populations", Opt. Lett. 3, 218-220, 1978.
[7] J. A. Miles, Z. J. Simmons, and D. D. Yavuz, "Subwavelength Localization of Atomic Excitation Using Electromagnetically Induced Transparency", Phys. Rev. X 3, 031014, 2013.
[8] K. Bergmann, H. Theuer, and B.W. Shore, "Coherent Population Transfer among Quantum States of Atoms and Molecules", Rev. Mod. Phys. 70, 1003, 1998.
[9] J. Gea-Banacloche, Y. Li, S. Jin, and M. Xiao, "Electromagnetically Induced Transparency in Ladder-type Inhomogeneously Broadened Media: Theory and Experiment", Phys. Rev. A 51, 576, 1995.
[10] A. Kasapi, M. Jain, G. Y. Yin, and S. E. Harris, "Electromagnetically Induced Transparency: Propagation Dynamics", Phys. Rev. Lett. 74, 2447, 1995.
[11] M. Xiao, Y. Li, S. Jin, and J. Gea-Banacloche, "Measurement of Dispersive Properties of Electromagnetically Induced Transparency in Rubidium Atoms", Phys. Rev. Lett. 74, 666, 1995.
[12] L. V. Hau, S. E. Harris, Z. Dutton, and C. H. Behroozi, "Light Speed Reduction to 17 m/s in an Ultracold Atomic Gas", Nature (London) 397, 594, 1999.
[13] M. M. Kash, V. A. Sautenkov, A. S. Zibrov, L. Hollberg, G.R. Welch, M.D. Lukin, Y. Rostovtsev, E.S. Fry, and M.O. Scully, "Ultraslow Group Velocity and Enhanced Nonlinear Effects in a Coherently Driven Atomic Gas", Phys. Rev. Lett. 82, 5229, 1999.
[14] Y. Rostovtsev, O. Kocharovskaya, G. R. Welch, and M. O. Scully, "Slow, Ultraslow, Stored, and Frozen Light", Opt. Photonics News 13, 44, 2002.
[15] G. M. Gehring, A. Schweinsberg, C. Barsi, N. Kostinski, and R.W. Boyd, "Observation of Backward Pulse Propagation through a Medium with a Negative Group Velocity", Science 312, 895, 2006.
[16] M. Fleischhauer and M. D. Lukin, "Dark State Polaritons in Electromagnetically Induced Transparency", Phys. Rev. Lett. 84, 5094, 2000.
[17] D. F. Phillips, A. Fleischhauer, A. Mair, R. L. Walsworth, and M. D. Lukin, "Storage of Light in Atomic Vapor", Phys. Rev. Lett. 86, 783, 2001.
[18] C. Liu, Z. Dutton, C. H. Behroozi, and L. V. Hau, "Observation of Coherent Information Storage in an Atomic Medium Using Halted Light Pulses", Nature (London) 409, 490, 2001.
[19] I. Novikova, A. V. Gorshkov, D. F. Phillips, A. S. Sorensen, M. D. Lukin, and R. L. Walsworth, "Optimal Control of Light Storage and Retrieval", Phys. Rev. Lett. 98, 243602, 2007.
[20] N. B. Phillips, A. V. Gorshkov, and I. Novikova, "Optimal Light Storage in Atomic Vapor", Phys. Rev. A 78, 023801, 2008.
[21] Julsgaard B., Sherson J., Cirac J. I., Fiurasek J. and Polzik E. S., "Experimental demonstration of quantum memory for light", Nature 432 482–6, 2004.

[22] Cho Y. W. and Kim. Y. H., "Storage and retrieval of thermal light in warm atomic vapor", Phys. Rev. A 82 033830, 2010.
[23] Cho Y. W. and Kim Y. H., "Atomic vapor quantum memory for a photonic polarization qubit", Opt Express 18 25786–93, 2010.
[24] Appel J., Figueroa E., Korystov D., Lobino M. and Lvovsky A., "Quantum memory for squeezed light", Phys. Rev. Lett. 100 093602, 2008.
[25] Höckel D. and Benson O., "Electromagnetically induced transparency in cesium vapor with probe pulses on the single-photon level", Phys. Rev. Lett. 105 153605, 2010.
[26] Riedl S., Lettner M., Vo C., Baur S., Rempe G. and Dürr S., "Bose–Einstein condensate as a quantum memory for a photonic polarization qubit", Phys. Rev. A 85 022318, 2012.
[27] Lettner M. et. al, "Remote entanglement between a single atom and a Bose–Einstein condensate", Phys. Rev. Lett. 106 210503, 2011.
[28] Zhang R., Garner S. R. and Hau L. V., "Creation of long- term coherent optical memory via controlled nonlinear interactions in Bose–Einstein condensates", Phys. Rev. Lett. 103 233602, 2009.
[29] Schraft D., Hain M., Lorenz N. and Halfmann T., "Stopped light at high storage efficiency in a Pr^{3+}: Y_2SiO_5 crystal", Phys. Rev. Lett. 116 073602, 2016.
[30] Chaneliere T., Matsukevich D., Jenkins S., Lan S. Y., Kennedy T. and Kuzmich A., "Storage and retrieval of single photons transmitted between remote quantum memories", Nature 438 833–6, 2005.
[31] Choi K. S., Deng H., Laurat J. and Kimble H. J., "Mapping photonic entanglement into and out of a quantum memory", Nature 452 67–U4, 2008.
[32] Zhang H. et. al, "Preparation and storage of frequency- uncorrelated entangled photons from cavity-enhanced spontaneous parametric down-conversion", Nat. Photonics 5 628–32, 2011.
[33] Bao X. H. et. al, "Efficient and long-lived quantum memory with cold atoms inside a ring cavity", Nat. Phys. 8 517–21, 2012.
[34] Chen Y. A. et. al, "Memory-built-in quantum teleportation with photonic and atomic qubits", Nat. Phys. 4 103–7, 2008.
[35] Radnaev A. G. et. al, "A quantum memory with telecom-wavelength conversion", Nat. Phys. 6 894–9, 2010.
[36] Akiba K., Kashiwagi K., Yonehara T. and Kozuma M., "Frequency-filtered storage of parametric fluorescence with electromagnetically induced transparency", Phys. Rev. A 76 023812, 2007.
[37] Akiba K., Kashiwagi K., Arikawa M. and Kozuma M., "Storage and retrieval of nonclassical photon pairs and conditional single photons generated by the parametric down-conversion process", New J. Phys. 11 013049, 2009.
[38] Zhou S. et. al, "Optimal storage and retrieval of single- photon waveforms", Opt. Express 20 24124–31, 2012.
[39] M. Fleischhauer and A. S. Manka, "Propagation of laser pulses and coherent population transfer in dissipative three-level systems: An adiabatic dressed-state picture", Phys. Rev. A 54, 794, 1996.
[40] J. Guo and J. Cooper, "Cooling and resonance fluorescence of two atoms in a one-dimensional optical molasses", Phys. Rev. A 51, 3128, 1995.
[41] A. V. Gorshkov, L. Jiang, M. Greiner, P. Zoller, and M. D. Lukin, "Coherent Quantum Optical Control with Subwavelength Resolution", Phys. Rev. Lett. 100, 093005, 2008.
[42] S. Harris, "Electromagnetically Induced Transparency", Physics Today, vol. 50, no. 7, pp. 36–42, 1997.